BIOCHEMISTRY
including biophysical chemistry & molecular biology

Article

pubs.acs.org/biochemistry

Loss of Electrostatic Interactions Causes Increase of Dynamics within the Plastocyanin–Cytochrome *f* Complex

Sandra Scanu,[†] Johannes M. Foerster,[†,‡] Monika Timmer,[†] G. Matthias Ullmann,[‡] and Marcellus Ubbink*[,†]

[†]Institute of Chemistry, Leiden University, Einsteinweg 55, 2333 CC Leiden, The Netherlands

[‡]Computational Biochemistry, University of Bayreuth, Universitätsstrasse 30, 95447 Bayreuth, Germany

Supporting Information

ABSTRACT: Recent studies on the electron transfer complex formed by cytochrome *f* and plastocyanin from *Nostoc* revealed that both hydrophobic and electrostatic interactions play a role in the process of complex formation. To study the balance between these two types of interactions in the encounter and the final state, the complex between plastocyanin from *Phormidium laminosum* and cytochrome *f* from *Nostoc* sp. PCC 7119 was investigated using NMR spectroscopy and Monte Carlo docking. Cytochrome *f* has a highly negative charge. *Phormidium* plastocyanin is similar to that from *Nostoc*, but the net charge of the protein is negative rather than positive. NMR titrations of Zn-substituted *Phormidium* plastocyanin and *Nostoc* cytochrome *f* indicated that a complex with an affinity intermediate between those of the *Nostoc* and *Phormidium* complexes is formed. Plastocyanin was found in a head-on orientation, as determined using pseudocontact shifts, similar to that in the *Phormidium* complex, in which the hydrophobic patch represents the main site of interaction on plastocyanin. However, the interaction in the cross-complex is dependent on electrostatics, similar to that in the *Nostoc* complex. The negative charge of plastocyanin decreases, but not abolishes, the attraction to cytochrome *f*, resulting in the formation of a more diffuse encounter complex than in the *Nostoc* case, as could be determined using paramagnetic relaxation spectroscopy. This work illustrates the subtle interplay of electrostatic and hydrophobic interactions in the formation of transient protein complexes. The results are discussed in the context of a model for association on the basis of hydrophobic contacts in the encounter state.

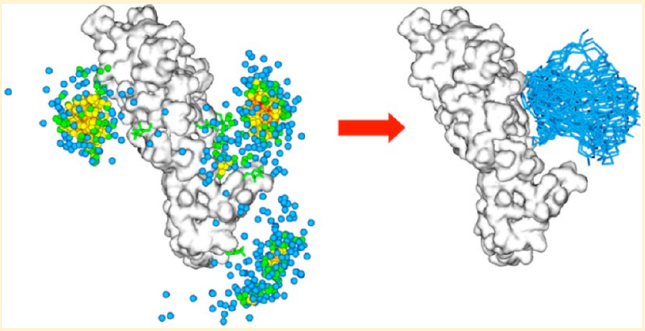

Protein association involves the formation of a dynamic encounter complex that is in equilibrium with the final, single-orientation complex.[1] In the encounter state, the proteins sample the surface of the partner, thus reducing the dimensionality of the search for the specific binding site.[2] Protein complex formation has been commonly described with a general model, in which the formation of the encounter complex is dominated by long-range electrostatic interactions, whereas the final state is determined by short-range interactions.[3] However, theoretical studies demonstrated that desolvation can be a dominant interaction in the process of complex formation for systems with weak charge complementarity.[4−6] Furthermore, partial desolvation of the binding interface was reported for some encounter complexes.[7,8] The recent characterization of the encounter state of cytochrome *f* (^{N}Cyt *f*) and plastocyanin (^{N}*Pc*) complex from the cyanobacteria *Nostoc* sp. PCC 7119 ($^{N-N}$complex) demonstrated experimentally that electrostatic interactions alone cannot describe the encounter complex, suggesting that hydrophobic interactions also contribute to its formation.[9] In the proposed model, long-range electrostatics result in the preorientation of ^{N}*Pc* relative to ^{N}Cyt *f*, and hydrophobic interactions stabilize the encounter complex by promoting the overlap of the extended nonpolar surfaces of both proteins. ^{N}*Pc* can diffuse in the hydrophobic interface and smoothly reach orientations capable of electron transfer (ET). The identification of hydrophobic interactions in the encounter state contrasts the view in which short-range interactions occur only in the final complex.[2]

Pc and Cyt *f* are photosynthetic redox partners in oxygenic organisms, such as plants, green algae, and cyanobacteria. *Pc* is a soluble electron carrier, which shuttles electrons from Cyt *f* of the cytochrome b_6f complex to photosystem I.[10−12] The association of *Pc* and Cyt *f* is on the border between electrostatic-assisted[13] and desolvation-mediated association,[4] therefore representing a good model to elucidate the balance between electrostatic and hydrophobic interactions in protein complex formation. *In vitro*, electrostatic interactions enable fast association,[14−19] and nonpolar interactions favor the stabilization of the complex in an ET active conformation.[20−22] The

Received: April 9, 2013
Revised: July 8, 2013
Published: August 28, 2013

dx.doi.org/10.1021/bi400450q | *Biochemistry* 2013, 52, 6615−6626

characterization of *Pc*-Cyt *f* complexes from several organisms revealed that small differences in the electrostatic surface properties of the proteins in the individual proteins strongly influence both the binding equilibrium and the final orientations of the complexes. Both in plants[20,23] and in the cyanobacteria *Nostoc*[22] and *Prochlorothrix hollandica*,[24] electrostatic interactions influence the final orientation of *Pc* with respect to Cyt *f* within the complex and tilt the long side of *Pc* toward the small domain of Cyt *f* in the so-called side-on orientation. The complex from the cyanobacterium *Phormidium laminosum* ($^{Ph\text{-}Ph}$complex) was found instead in the head-on orientation, in which solely the hydrophobic ET site represents the binding site.[21] Neutralization of charged residues on the surface of ^{Ph}Pc[16] and ^{N}Pc[18] has shown to have greater effect on the kinetics of the reaction than similar modifications on ^{Ph}Cyt *f*[17] and ^{N}Cyt *f*,[19] respectively. ^{Ph}Cyt *f* and ^{N}Cyt *f* are electrostatically similar, with an overall charge of −13 and −15,[25] respectively, and a rather even distribution of the negative charges over the surfaces. The two *Pc*'s show 63% amino acid sequence identity and very similar three-dimensional structures, but they vary considerably in their electrostatic properties. ^{N}Pc is overall positively charged with six lysines (K6, K11, K20, K24, K35, and K100) forming an extended charged patch, which juxtaposes the long side of ^{N}Cyt *f* in the side-on orientation. In ^{Ph}Pc, K11 and K20 are substituted by serine and asparagine, respectively, and the positively charged patch is composed of four lysines (K6, K30, K35, and K100), yielding a protein with a net negative charge (−1 at pH 6). To evaluate the effects that these electrostatic differences between the two *Pc*'s can cause along the association pathway of Cyt *f* and *Pc*, the complex of ^{N}Cyt *f* and ^{Ph}Pc ($^{N\text{-}Ph}$complex) was studied using NMR spectroscopy and computational approaches. The consequences for binding affinity, final complex orientation, and encounter complex are discussed in light of the recent findings for the $^{N\text{–}N}$complex.[9]

EXPERIMENTAL SECTION

Protein Production and Purification. The plasmid pET11PC,[26] which contains the gene for wild-type ^{Ph}Pc, was transformed in *E. coli* BL21 pLysS. ^{15}N enriched-Zn substituted *Pc* was produced as described before for ^{N}Pc,[27] with the difference that ampicilline (100 mg/L) and chloramphenicol (20 mg/L) were added to the growth media instead of kanamycin. The purification procedure was reported before.[21] The concentration of the protein was determined by absorbance spectroscopy using ε_{280} = 5 $mM^{-1}cm^{-1}$. The yield of pure protein was 4 mg/L of culture.

The pEAF-WT plasmid, containing the gene of the soluble domain (residue 1−254) of *Nostoc* sp. PCC 7119 Cyf *f* was kindly provided by Professor Dr. Miguel A. De la Rosa (University of Seville). Cyt *f* mutants were obtained using pEAF-WT plasmid as template for mutagenesis as described before.[9,27,28] Production and purification of the protein and spin label attachment were performed as previously reported.[9,18,27]

NMR Experiments. All NMR samples contained 2-(*N*-morpholino) ethanesulfonic acid (MES, 20 mM, pH 6) and 6% D_2O for lock. The pH of the sample was adjusted with small aliquots of HCl (0.5 M) and NaOH (0.5 M). For the chemical shift perturbation (CSP) experiments, Cyt *f* was titrated into Zn-substituted ^{15}N *Pc* (40 μM). Spectra were recorded at multiple Cyt *f*/*Pc* molar ratios (0.1, 0.2, 0.4, 0.6, 0.8, 1.0, 2.5, 5.0, 7.5, and 10). For measurements of the pseudocontact shifts (PCSs), HSQC spectra of the free *Pc* and in the presence of ferric and ferrous Cyt *f* were acquired on the same sample. Ferric Cyt *f* was oxidized with $K_3[Fe(CN)_6]$ and loaded on a PD10 column to remove the oxidant, concentrated, and then added to *Pc* (final concentration of 135 μM) to a Cyt *f*/*Pc* molar ratio of 3:1. Ferric Cyt *f* was then reduced by adding 10 mol equiv of ascorbic acid directly into the sample. For the paramagnetic relaxation enhancement (PRE) experiments, the ferric state of Cyt *f* was preserved by the addition of $K_3[Fe(CN)_6]$ (50 μM). These samples contained 135 μM Cyt *f* for the Q125C mutant and 300 μM for the other mutants, labeled with either (1-acetoxy-2,2,5,5-tetramethyl-δ-3-pyrroline-3-methyl) methanethiosulfonate (MTS) or (1-oxyl-2,2,5,5-tetramethyl-δ-3-pyrroline-3-methyl) methanethiosulfonate (MTSL). Samples also contained Zn-substituted ^{15}N *Pc*, 45 μM in the sample with Q125C Cyt *f*, and 100 μM for the other Cyt *f* mutants. All NMR spectra were recorded at 298 K on a Bruker Avance III 600 MHz spectrometer equipped with a TCI-Z-GRAD CryoProbe. The $^{1}H-^{15}N$ HSQC spectra were acquired with 1024 and 80 complex points in the direct and indirect dimensions, respectively.

NMR Data Analysis. The NMR spectra were processed with NmrPipe[29] and analyzed with CcpNMR Analysis.[30] CSP analysis was carried out as described before.[27] PCS was defined as the chemical shift difference for a resonance in the presence of paramagnetic and diamagnetic Cyt *f*, according to previously reported procedures.[20,22]

The PREs were determined according to the procedure described by Battiste and Wagner.[31] The intensity ratio I_p/I_d of the *Pc* resonances in the presence of MTSL-Cyt *f* (I_p) and MTS-Cyt *f* (I_d) were normalized by dividing them by the average value of the 10 largest I_p/I_d values (1.09 for Q7C, 1.05 for Q38C, 2.21 for N71C, 1.41 for Q125C, 1.16 for S181C, and 1.25 for S192). The PRE (Γ_2) values were calculated according to eq 1:

$$\frac{I_p}{I_d} = \frac{R_{2d}\exp(-\Gamma_2 t)}{R_{2d} + \Gamma_2} \quad (1)$$

R_{2d} represents the transverse relaxation rate in the diamagnetic sample, which was calculated from the line width at half height obtained from a Lorentzian peak fit in the direct dimension by using FuDA (this software was kindly provided by Dr. D. Fleming Hansen, University College London). The symbol *t* indicates the time for transverse relaxation during the pulse sequence (9 ms). The Γ_2 values were extrapolated to the 100% bound state using the experimentally obtained K_D. The uncertainty for I_p/I_d ratios ($\Delta\sigma_{Ip/Id}$) was determined by error propagation according to eq 2 in which σ_p and σ_d represent the noise level of paramagnetic and diamagnetic spectra, respectively.:

$$\Delta\sigma_{I_p/I_d} = \frac{I_p}{I_d}\sqrt{\left(\frac{\sigma_p}{I_p}\right)^2 + \left(\frac{\sigma_d}{I_d}\right)^2} \quad (2)$$

The noise level of each spectrum is represented by the standard deviation of the intensities measured at 10 randomly chosen positions on the baseline.

Docking Calculations. The structure of the soluble part of Cyt *f* (residues 1−254) used for the calculation was taken from PDB entry 2ZT9[32] as described before.[27] The structure of ^{Ph}Pc was taken from PDB entry 2Q5B. The orientation of ^{Ph}Pc in complex with ^{N}Cyt *f* was determined by rigid body docking

dx.doi.org/10.1021/bi400450q | *Biochemistry* 2013, 52, 6615−6626

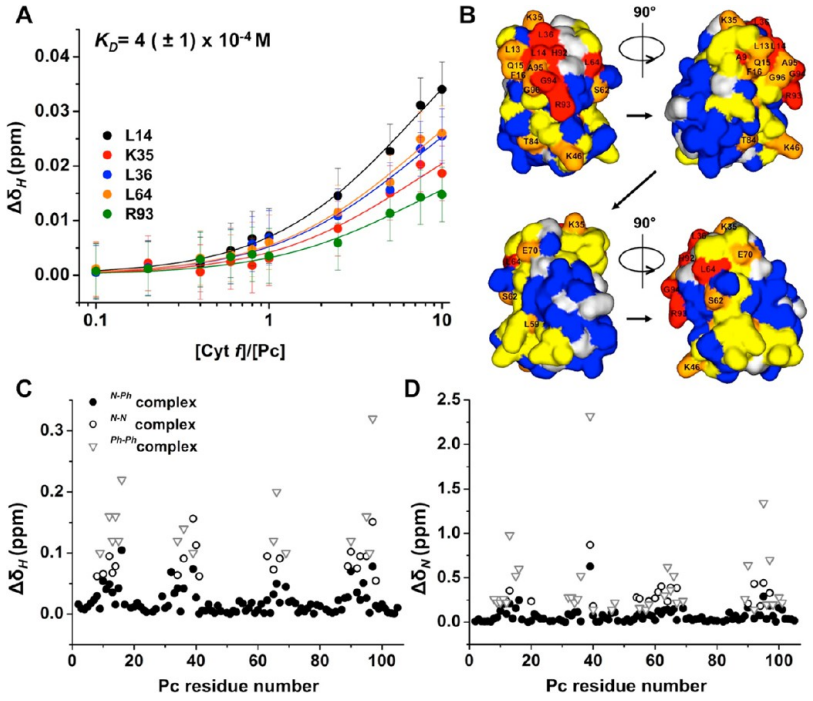

Figure 1. Interaction of Zn-substituted ^{15}N ^{Ph}*Pc* with ^{N}Cyt *f*. (A) CSP curves for Zn ^{Ph}*Pc* binding to ^{N}Cyt *f* for selected residues fitted to a 1:1 interaction model. (B) Binding map of ^{Ph}*Pc* in the presence of wild-type ^{N}Cyt *f* (Fe III), color-coded on a surface model of *Pc* (PDB entry 2Q5B). The red color corresponds to $\Delta\delta_{AVG} \geq$ 0.030 ppm, orange to $\Delta\delta_{AVG} \geq$ 0.015 ppm, yellow to $\Delta\delta_{AVG} \geq$ 0.0075 ppm, and blue to $\Delta\delta_{AVG} \leq$ 0.0075 ppm. Prolines and overlapping residues are colored in light gray. This image and others of molecular structures were made with Discovery Studio Visualizer 2.5 (Accelrys). (C,D) Chemical shift perturbations of ^{Ph}*Pc* resonances upon the binding of ^{N}Cyt *f* (Fe II). The CSPs in ^{1}H dimension (C) and in ^{15}N dimension (D) observed for the $^{N\text{-}Ph}$complex are shown as black dots, for the $^{N\text{–}N}$complex as black circles, and for $^{Ph\text{-}Ph}$complex as gray triangles.

using solely PCS restraints with the option PARAstraints[33] in Xplor-NIH 2.9.9.[34] For this reason, the observed ^{1}H$\Delta\delta_{PCS}$ were extrapolated to 100% bound *Pc* by dividing them by the fraction bound (0.47). The size of the axial magnetic component of the magnetic susceptibility anisotropy tensor ($\Delta\chi_{ax}$) was derived from the g-tensor values measured by EPR spectroscopy on plant Cyt *f* (7×10^{-32} m^3).[22] However, the value required to obtain convergence of the structure calculations is much smaller. One reason for this is the temperature difference between the EPR measurements (10 K) and NMR spectra (taken at 298 K). The second reason is an averaging effect occurring in the encounter state, which reduces the PCS considerably. The $\Delta\chi_{ax}$ was varied in the range ($0.61–3.3$) $\times 10^{-32}$ m^3. The best convergence was found for $\Delta\chi_{ax}$ = 0.87×10^{-32} m^3, whereas it was taken to be 3.8×10^{-32} m^3 in the $^{N\text{–}N}$complex.[22] The intermolecular PCSs from the ferric heme iron of Cyt *f* to the backbone amide atoms in *Pc* were back-calculated from the best 20 structures and compared with the experimental PCSs. Equation 3 was used for the PCS calculation, assuming an axial magnetic susceptibility tensor oriented along the vector defined by the iron and the N-atom of Y1 of Cyt *f*:[20]

$$\Delta\delta_{PCS} = \frac{\Delta\chi_{ax}}{12\pi r^3}(3\cos^2\theta - 1) \quad (3)$$

In eq 3, $\Delta\delta_{PCS}$ is the PCS, *r* is the distance between the heme iron and the observed *Pc* nucleus, and θ is the angle among the *Pc* nucleus, heme iron, and the nitrogen of the amine group of Y1 in Cyt *f*. The degree of agreement between observed (PCS^{obs}) and back-calculated (PCS^{calc}) PCSs was determined by the PCS Q factor, defined as follows:

$$Q_{PCS} = \sqrt{\frac{\sum (PCS^{obs} - PCS^{calc})^2}{\sum (|PCS^{obs}| + |PCS^{calc}|)^2}} \quad (4)$$

Ensemble docking was performed as described for the $^{N\text{–}N}$complex with seven *Pc* copies per docking.[9] The restraints for the calculations were obtained according to equation 5:

$$\Gamma_2^{obs} = f_1\Gamma_2^{ens} + f_2\Gamma_2^{final} \quad (5a)$$

$$f_1 + f_2 = 1 \quad (5b)$$

The ensemble Γ_2 (Γ_2^{ens}) was calculated as the difference between observed Γ_2 (Γ_2^{obs}) and average back-calculated Γ_2 from the models of the PCS-based final complex (Γ_2^{final}). The calculations were carried out with f_2 values = 0, 0.15, 0.25, 0.35, 0.5, 0.65, 0.75, 0.85, 0.95, and 1. The restraints were grouped into three classes as described before.[27] For the visualization of the encounter complex ensemble, 150 docking runs were performed, yielding 148 ensembles of 7 *Pc* conformers, with a difference in the total restraint energy ≤20%.

The ensembles from separated dockings were evaluated by means of the averaged violation for all experimental restraints as described before.[9]

Monte Carlo Simulations of the Encounter Complex. The structure files for Cyt *f* and *Pc* were taken from the PDB entries 2ZT9[32] and 2Q5B, respectively. Monte Carlo (MC) simulations generate a Boltzmann distribution of encounter complexes according to their electrostatic interaction energy.[35] The simulations were performed using a previously described approach.[9,36]

dx.doi.org/10.1021/bi400450q | *Biochemistry* 2013, 52, 6615–6626

RESULTS AND DISCUSSION

Affinity and Binding Site. For the characterization of the nonphysiological cyanobacterial $^{N\text{-}Ph}$complex formed by ^{N}Cyt *f* and ^{Ph}*Pc*, ^{15}N-enriched Zn-^{Ph}*Pc* was titrated to either oxidized ^{N}Cyt *f* (Fe^{III}) or reduced ^{N}Cyt *f* (Fe^{II}) to molar ratios *Pc*/Cyt *f* 1:10 and 1:3, respectively. ^{Ph}*Pc* was produced with Zn rather than the Cu in the binding site to avoid the effects of ET and the disappearance of important resonances due to the line-broadening caused by the paramagnetic Cu.[37] Each titration point was monitored through the acquisition of $^{15}N-^{1}H$ HSQC spectra. Upon addition of Cyt *f*, a number of resonances shifted in the spectrum, indicating complex formation. The appearance of shifting resonances indicates that free and bound *Pc* are in fast exchange on the NMR time scale. The binding curves for the most affected residues were obtained by plotting the chemical shift perturbation (CSP, $\Delta\delta_H$) versus Cyt *f*(Fe^{III})/*Pc* molar ratio, as shown in Figure 1A.

The CSP curves did not reach saturation, indicating a low affinity. The global fit of the binding curves to a 1:1 binding model yielded a dissociation constant of 4 ($\pm$1) $\times$ 10^{-4} M. This value is in-between the reported values for the $^{Ph\text{-}Ph}$complex and $^{N-N}$complex, being $\approx$10 $\times$ 10^{-4} M[21] and 0.8 $\times$ 10^{-4} M,[27] respectively. Whereas the cross-complex formed by ^{Ph}Cyt *f* and ^{N}*Pc* ($^{Ph\text{-}N}$complex) was reported to have similar affinity to the $^{N-N}$complex (K_D = 0.8 $\times$ 10^{-4} M),[25] the $^{N\text{-}Ph}$complex shows an affinity intermediate to that of the two physiological complexes but closer to that of the $^{Ph\text{-}Ph}$complex. The experimental K_D was used to determine whether the fraction of ^{Ph}*Pc* bound to ^{N}Cyt *f* at the last point of the titration was 0.52, and the average amide CSPs ($\Delta\delta_{AVG}$) were extrapolated to the 100% bound form. The CSP map of Zn-^{Ph}*Pc* was obtained by color coding each residue according to the size of $\Delta\delta_{AVG}$ (Figure 1B). The largest effects were observed for residues surrounding the metal binding site, namely, A9, L14, L36, H39, L64, H92, R93, and G94, colored in red. Most of these residues are hydrophobic and make up the hydrophobic patch of *Pc*, which was also identified as the main binding site in the structural models of the $^{N-N}$complex and $^{Ph\text{-}Ph}$complex.[21,22] Clearly, the hydrophobic patch plays a fundamental role in the formation of the Cyt *f*-*Pc* complexes. The CSP map is qualitatively similar to that of the $^{N-N}$complex[22,27] with a prominent perturbation for R93, known to be involved in the binding in both the $^{N-N}$complex[18,19,22] and $^{Ph\text{-}Ph}$complex.[16] Interestingly, a significant CSP was also observed for K46 in the $^{N\text{-}Ph}$complex. K46 is located far from the hydrophobic patch, well below R93, and kinetic studies suggested its involvement in the electrostatic modulation of the binding of $^{Ph\text{-}Ph}$complex.[16]

Structure of the Final Complex. The orientation of the ^{Ph}*Pc* in complex with ^{N}Cyt *f* was determined by taking advantage of the intermolecular PCSs caused by the paramagnetic oxidized iron of Cyt *f* on *Pc* backbone amide protons, in a way similar to that done previously for other *Pc*-Cyt *f* complexes.[20,21,23,24] PCSs arise from the through-space interaction between the spin of the unpaired electron and that of the observed nucleus. PCS is distance and orientation dependent and provides restraints for structural calculations. The calculations converged to an ensemble of structures. The best 20 structures exhibit a difference in the restraint energy of less than 6% and are shown in Figure 2A.

The resulting model shows a high degree of variability, but in all structures, the hydrophobic patch of *Pc* is making contact with the hydrophobic patch surrounding the heme of Cyt *f* and

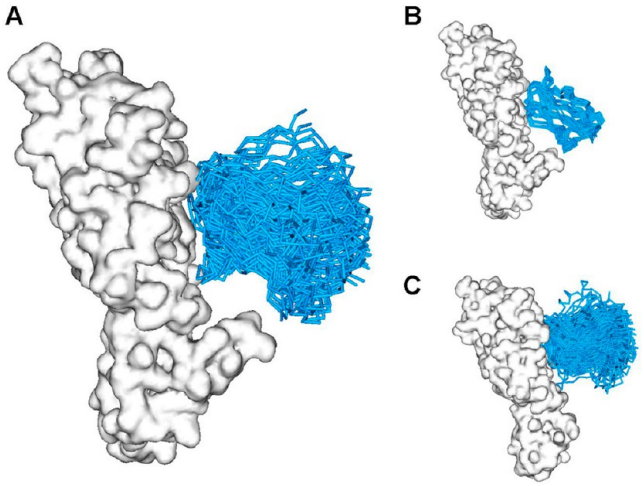

Figure 2. Comparison of the structures of *Pc*-Cyt *f* complexes, showing the structure obtained for the $^{N\text{-}Ph}$complex (A), the physiological $^{N-N}$complex (PDB entry 1TU2[22]) (B), and $^{Ph\text{-}Ph}$complex (C).[21] ^{N}Cyt *f* and ^{Ph}Cyt *f* are shown as white surface models of PDB entries 2ZT9 and 1CI3,[38] respectively, and *Pc* is represented by the ensemble of the 20 (A), 10 (B), and 25 (C) lowest energy conformations, shown as cyan C_α traces.

represents the entire complex interface. All structures showed an interaction between H92 of *Pc* and F3 of Cyt *f*, also found in the $^{Ph\text{-}Ph}$complex[21] and $^{N-N}$complex.[22] The binding interface is composed of polar and hydrophobic residues, located in the regions 11–14, 36–39, 64–68, and 90–95 on ^{Ph}*Pc*. R93 represents the only charged interfacial residue. The averaged Cu–Fe distance in the ensemble was 15.3 ($\pm$0.5) Å. In Figure 3A, the observed (black dots) and the back-calculated PCSs for the best 20 structures (gray lines) are plotted versus *Pc* residue numbers.

For most residues, experimental and back-calculated PCSs agree within the error margins. Small deviations are observed for F16, V29, W31, V32, and A90, which form the edge of the hydrophobic binding site, and M97, which coordinates the metal. Considering the relative vicinity of these residues to the heme, it is possible that the approximations made for the size, axiality, and orientation of the magnetic susceptibility tensor cause these deviations. The overall quality of the structures was evaluated by calculating a quality (Q) factor for the back-calculated PCSs for each structure of the final model and the experimental PCSs (see Experimental Section, eq 4). The average Q value was calculated to be 0.23 ($\pm$0.01).

The orientation of *Pc* in the complex is more similar to the head-on orientation found in the $^{Ph\text{-}Ph}$complex (Figure 2C) than to the side-on orientation of the $^{N-N}$complex (Figure 2B). ^{Ph}*Pc* is oriented perpendicular to the heme with a slight tilt toward the small domain of ^{N}Cyt *f*. In the $^{N-N}$complex, the specific electrostatic contacts between K57 and K62 of ^{N}*Pc* and E189 and D64 of ^{N}Cyt *f* appear to be responsible for the long side of *Pc* to be tilted toward Cyt *f*.[22,25] In ^{Ph}*Pc*, these lysines are substituted with D57 and S62, respectively, and the loss of these important electrostatic contacts may lead to the head-on orientation in the $^{N\text{-}Ph}$complex. In the $^{N\text{-}Ph}$complex, only the bottom part of ^{Ph}*Pc* (relative to the hydrophobic patch) is turned toward the small domain of ^{N}Cyt *f*, probably as a consequence of the charge–charge interaction between K46 of ^{Ph}*Pc* and E189 and D190 of ^{N}Cyt *f*. The soluble part of ^{Ph}Cyt *f* is shorter than ^{N}Cyt *f*, comprising 249 instead of 254 residues.

dx.doi.org/10.1021/bi400450q | *Biochemistry* 2013, 52, 6615–6626

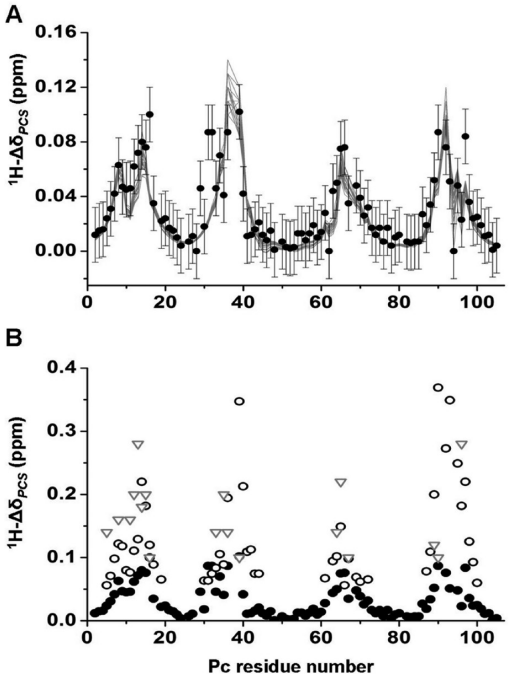

Figure 3. Evaluation of $^{N\text{-}Ph}$complex. In panel A, the observed ^{1}HΔδ_{PCS}, which were extrapolated to 100% bound *Pc*, are shown as black dots, and the back-calculated ^{1}HΔδ_{PCS} for the 20 lowest PCS energy structures are shown as gray lines. The error bars represent the estimated experimental errors in the resonance positions. In panel B, the observed ^{1}HΔδ_{PCS} for the $^{N\text{-}Ph}$complex are shown as black dots, for the $^{N-N}$complex[22] as black circles, and for the $^{Ph\text{-}Ph}$complex[21] as gray triangles. All PCSs were extrapolated to the 100% bound form and plotted versus *Pc* residue numbers.

This causes the small domain to be less extended and not in direct contact with *Pc* in the $^{Ph\text{-}Ph}$complex.[21] In the $^{N\text{-}Ph}$complex, K46 is in a favorable position to have electrostatic interactions with E189 and D190 in the prominent small domain of Cyt *f*.

Since PCSs depend on the orientation of the observed nucleus with respect to the paramagnetic iron, the presence of multiple orientations is expected to influence the size of PCSs. In the *Pc*-Cyt *f* complex from *Prochlorothrix hollandica*, the mutation of Y12 and P14 in *Pc* to Gly and Leu, respectively, caused an increase of dynamics, as judged by the decrease of PCSs for nuclei in certain regions of *Pc*.[24] In Figure 3B, the observed ^{1}HΔδ_{PCS} of the $^{N\text{-}Ph}$complex were compared with the reported values for the $^{N-N}$complex[22] and $^{Ph\text{-}Ph}$complex,[21] each extrapolated to the 100% bound state. The pattern of the ^{1}HΔδ_{PCS} is similar for all complexes, but the sizes of ^{1}HΔδ_{PCS} are comparable only for the two physiological complexes, whereas they are considerably lower for the $^{N\text{-}Ph}$complex. This indicates that in the $^{N\text{-}Ph}$complex the dynamics of *Pc* is larger than that in both the $^{N-N}$complex and the $^{Ph\text{-}Ph}$complex.

Encounter Complex. To map the distribution of the encounter intermediates on the ^{N}Cyt *f* surface in the $^{N\text{-}Ph}$complex, six spin labels were attached on ^{N}Cyt *f*, one at a time, and PREs were measured on the amide backbone protons of ^{Ph}*Pc*. Cyt *f* was added to *Pc* in a molar ratio *Pc*/Cyt *f* of 1:3. PRE causes line broadening of *Pc* resonances resulting in a low ratio of peak intensities in the spectra of the paramagnetic and diamagnetic samples (I_p/I_d). In Figure 4 (central panel), the positions of spin labels are shown on a surface model of Cyt *f* with respect to *Pc* oriented as found in the lowest energy structure of the PCS-based final complex (cyan C_α trace). Spin labels attached to Cyt *f* on the same side as the binding site for *Pc*, at positions Q7, N71, and S192, caused a large decrease of I_p/I_d ratios of *Pc* resonances.

It is noteworthy also that spin labels attached on the backside of Cyt *f*, at the positions Q38 and Q125, or located far away, S181, showed a moderate to large decrease for some resonances. The large error bars calculated for the ratios in the presence of the Q125C mutant are due to the lower concentration of *Pc* in this sample (45 μM) as compared to that in the other mutants (100 μM) resulting in a low signal-to-noise ratio. The I_p/I_d ratios were used to determine the PRE (Γ_2). In the fast exchange regime (see above), the observed PREs are weighted averages of free *Pc*, the encounter complex, and the final complex. The PREs were extrapolated to the 100% bound state (encounter complex + final complex) by dividing by the fraction of bound *Pc*. The PREs caused by each spin label were mapped on the surface of *Pc* (Figure 5).

Even though the three spin labels located at the same side of Cyt *f* as the binding site (Q7C, N71C, and S192C) are relatively far from each other, the PRE patterns are very similar and resemble the CSP map in the presence of wild-type Cyt *f* (Figure 1B). The qualitative similarity of the PRE patterns suggests that *Pc* samples a large area of the Cyt *f* surface, while maintaining the same relative orientation to Cyt *f*. The highest PREs were observed for residues located in the hydrophobic patch of *Pc*, indicated as main binding site in the PCS-based final complex. Most of these residues are hydrophobic or polar, with the exception of R93 that was strongly affected by PRE in the presence of spin labels in N71 and S192. The same residue exhibited a high CSP in the presence of wild-type Cyt *f* (Figure 1B). Interestingly, for most of these residues moderate PREs were also observed in the presence of spin labels attached to the backside of Cyt *f* with respect to the PCS-based binding site of *Pc*, indicating that *Pc* also visits this part of Cyt *f*.

The encounter complex was visualized by ensemble docking. This approach is based on the fact that PREs result from the weighted average contribution of all species in solution, both the encounter and the final complexes.[39] To represent all species that contribute to the observed PREs, multiple conformers of a protein are simultaneously docked on the other protein to obtain a population distribution that fits the experimental data. Each docking yields a unique ensemble of orientations that account for the experimental PREs. To separate the PRE contribution of the complex in the final state, the averaged back-calculated PREs from the PCS-based models of the final complex were subtracted from experimental PREs, and the resulting PREs were used. A series of ensemble docking calculations were then carried out by varying the population of the final state (f_2) from 1 to 0. The resulting ensembles were evaluated by calculating the average distance violation over all experimental distances. The average distance violations were plotted versus the percentage of the encounter complex (Figure S1, Supporting Information). The violations show that the observed PREs are not explained by the PCS-based structure alone. A significant decrease in the average violation is already observed when the encounter complex is taken to be 5%. Further increase of the encounter complex fraction in the restraints did not improve the fit of the data. For all generated ensembles, an average violation of about 2 Å was observed.

The calculations for the representation of the encounter complex were performed assuming a pure encounter state (f_1 = 1). The comparison of the back-calculated distances between the oxygen atom of the spin labels and the amide protons of all

dx.doi.org/10.1021/bi400450q | *Biochemistry* 2013, 52, 6615−6626

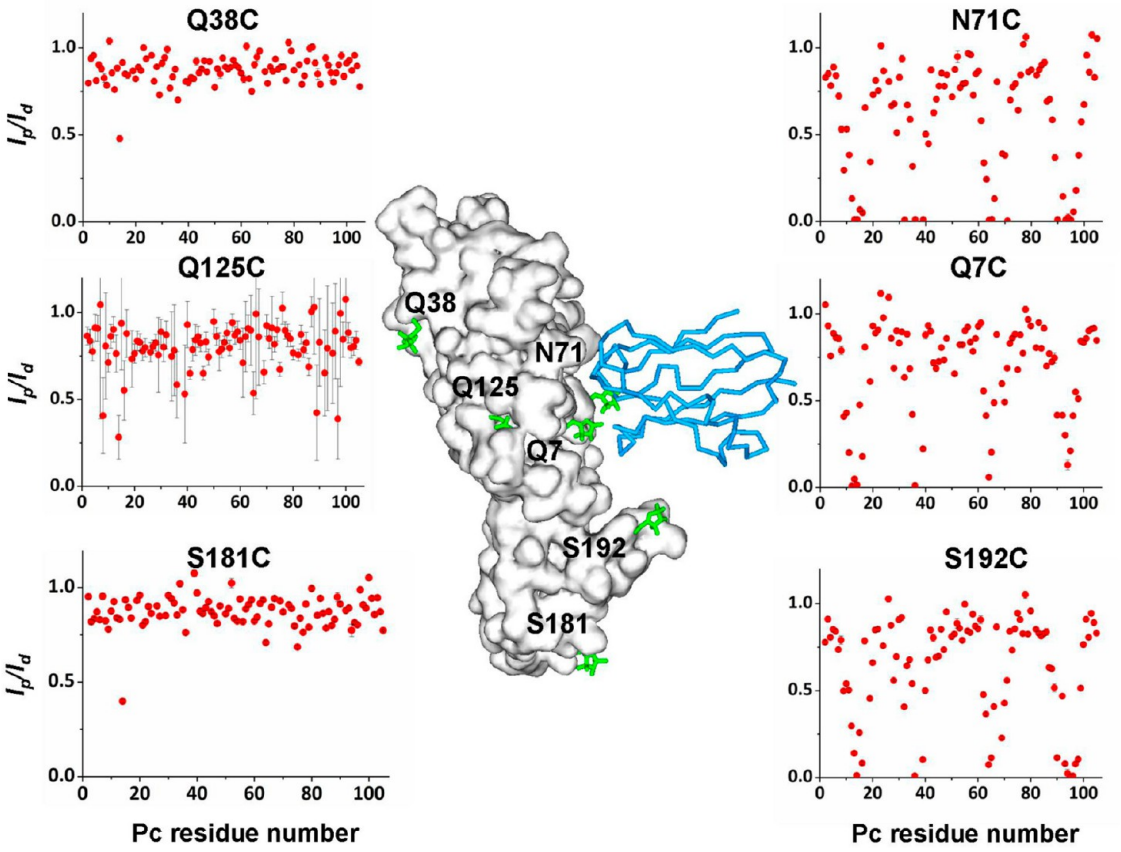

Figure 4. PRE in the $^{N\text{-}Ph}$complex. Central panel: location of the spin labels (green sticks) modeled on the ^{N}Cyt *f* (PDB entry 2ZT9). Cyt *f* is shown as a white surface, and *Pc* is represented as a cyan C_α trace, oriented as the PCS-based final complex. Side panels: the I_p/I_d ratios are plotted versus the *Pc* residue number for each of the spin label positions on Cyt *f*. The error bars represent the uncertainty for I_p/I_d ratios based on the noise levels of the spectra. For most points, the error bar is within the symbol.

Pc conformers of the generated encounter complex (red line in Figure 6) and the back-calculated distances in the PCS-based models of the final complex (blue line) shows that only the generated encounter complex fits the experimental distances (green dots and line).

The main deviation is represented by S192C, indicating that ^{Ph}*Pc* spends more time close to this spin label than expected from the PCS-based models. This suggests that PREs from S192C mainly arise from the encounter complex. Most of calculated distances from the generated encounter complex lie within the error margins of the experimental values. Deviations were observed for the spin label Q125C, likely due to the poor data quality (see above).

To represent the encounter complex, an ensemble from 145 docking solutions, with a total of 1015 *Pc* conformers was generated (Figure 7A).

The centers of mass (CoMs) of *Pc* were colored according to the density of distribution, with red and blue representing the largest and smallest densities, respectively. It should be noted that the incomplete coverage of spin labels on the Cyt *f* surface implies that also other Cyt *f* surface areas could be involved in the encounter complex. The current analysis shows that the encounter complex is at least distributed over three extensive areas of Cyt *f* surface. The most extended area is located in the vicinity of the binding site found in the final complex models, the second is in front of the small domain of Cyt *f*, and the third on the backside relative to the final complex. The third area is an artifact due to the use of the soluble part of ^{N}Cyt *f*. *In vivo*, Cyt *f* is embedded on the thylakoid membrane that will prevent *Pc* from binding on this side.[9] In all three areas, the interface comprises large patches of polar and hydrophobic residues. Despite the fact that in this study a less extensive portion of the Cyt *f* surface was monitored, the encounter complex resembles the one found for the $^{N-N}$complex (Figure 7B). The encounter ensemble of $^{N\text{-}Ph}$complex is more extensive and covers a larger area of the hydrophobic regions of Cyt *f*. In the $^{N-N}$complex, stronger charge interactions may lead to more defined encounter regions. In the $^{N-N}$complex, one continuous diffusive encounter region is present on the side of the binding site, while in the $^{N\text{-}Ph}$complex, two distinct diffusive encounter areas can be seen. To evaluate the distribution of the ET active complexes, the CoMs of ^{Ph}*Pc* are colored according to the calculated distance between Cu in *Pc* and Fe in Cyt *f*, with red and blue representing the smallest and largest distances, respectively (Figure S2A, Supporting Information). As for the $^{N-N}$complex (Figure S2B, Supporting Information), the encounter complex orientations compatible with rapid ET (red dots, Cu−Fe distance ≤16 Å) are located only in front of the heme, in close vicinity of the binding site found in the final complex.

Role of Electrostatic Interactions in Complex Formation. The effect of ionic strength (*I*) on the binding shifts of ^{Ph}*Pc* in the presence of reduced ^{N}Cyf *f* at a Cyf *f*/*Pc* molar ratio of 3:1 was investigated at NaCl concentrations of 100 mM (*I* = 110 mM) and 200 mM (*I* = 210 mM). The CSPs ($\Delta\delta_H$) were defined relative to the control measurements recorded on free

dx.doi.org/10.1021/bi400450q | *Biochemistry* 2013, 52, 6615−6626

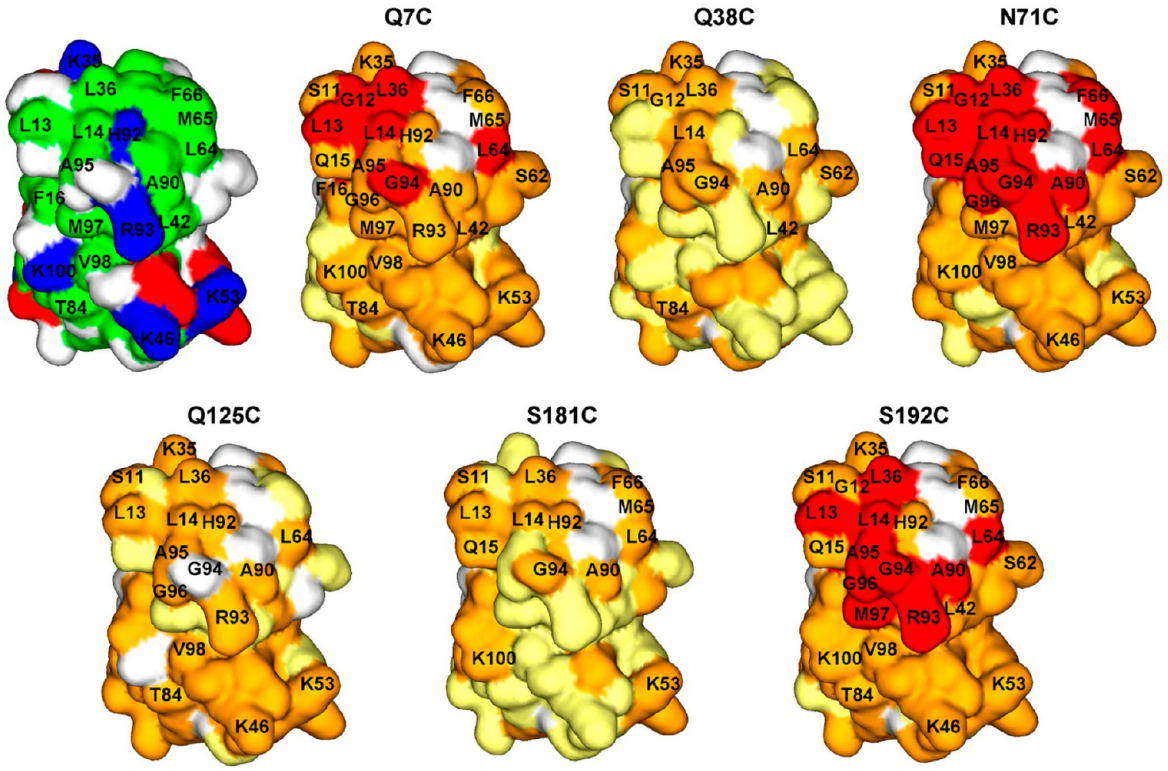

Figure 5. PRE maps of ^{15}N enriched Zn-substituted ^{Ph}*Pc* in the presence of MTSL-conjugated ^{N}Cyt *f*, color-coded on a surface model of *Pc* (PDB-entry 2QSB). Experimental PREs were extrapolated to 100% bound *Pc*. Residues with $\Gamma_2 \geq 200$ s^{-1} are colored in red, with 10 s^{-1}< Γ_2< 200 s^{-1} in orange and with $\Gamma_2 \leq 10$ s^{-1} in light yellow. Prolines and residues with overlapping resonances are colored in white. On the top left, *Pc* is colored according to its charge distribution. Negatively and positively charged residues are shown in red and blue, respectively. Hydrophobic residues are in green and polar residues in white.

^{Ph}*Pc* at the same NaCl concentration. The $\Delta\delta_H$ values at the different salt concentrations were plotted versus ^{Ph}*Pc* residue numbers (Figure 8A).

The addition of 200 mM NaCl did not affect the perturbation pattern observed in the absence of salt. The residues showing the strongest ionic strength dependence, namely, V15, F16, V32, L36, H39, A90, and M97, are located in the loops that make up the hydrophobic patch. Similarly to what was observed for the $^{N-N}$complex,[25] all major shifts ($\Delta\delta_H \geq 0.03$ ppm) decreased by about 60% upon the addition of 200 mM NaCl. These findings suggest that at low ionic strength favorable electrostatic interactions play a role also in $^{N\text{-}Ph}$complex formation but do not influence the relative orientation of the proteins within the final complex. Apparently, attractive interactions exist despite the fact that ^{N}Cyt *f* and ^{Ph}*Pc* both have an overall negative charge at pH 6. This observation suggests that charge distribution plays a critical role in the association process at low ionic strength. For this reason, MC simulations were performed.

In rigid-body MC simulations, the association of two proteins is simulated on the basis of their electrostatic potentials.[35] On the assumption that the formation of the encounter complex is purely driven by long-range electrostatic forces,[2] PRE and MC simulations were successfully combined for the visualization of the encounter complex of cytochrome *c* and cytochrome *c* peroxidase, demonstrating that the formation of this complex could be explained by electrostatic interactions alone.[36] The same approach on the $^{N-N}$complex was revealed to be inadequate to describe the encounter complex, which appears to be stabilized by electrostatic as well as hydrophobic interactions.[9] At the same time, MC simulations provided evidence of the electrostatic preorientation of *Pc* toward Cyt *f*, as was found on the basis of CSP and PRE data. MC simulations were performed for the $^{N\text{-}Ph}$complex to establish whether electrostatic preorientation of ^{Ph}*Pc* can occur despite the negative charge of both proteins. The calculations produced an ensemble consisting of the Boltzmann distribution of orientations of Cyt *f* around *Pc*. An ensemble of 5000 structures was randomly selected from the entire set of two million solutions, and the positions of Cyt *f* CoMs were plotted in Figure 8C. The position in the plot is determined by two angles. The first is the cone angle (α) formed by the Cyt *f* CoM, the *Pc* CoM, and the Nε atom of copper ligand H92, taken as the center of the hydrophobic patch. The larger this angle is, the further the Cyt *f* CoM is rotated away from the hydrophobic patch. The α angle is represented by the circles in Figure 8C and D. The second angle, β, indicates the position on the cone and represents the side of *Pc* to which the Cyt *f* CoM is rotated. The hydrophobic patch is delineated by a red line marked with residue numbers. Figure 8C shows that Cyt *f* binds in a diffusive manner but more toward the hydrophobic patch side of ^{Ph}*Pc* than toward the other end. Clearly, preorientation occurs due to electrostatic interactions. This finding is also illustrated in Figure 8B. The cumulative fraction of Cyt *f* CoMs for the α angle is plotted (black bars). The red line represents the cumulative fraction for a completely random distribution around a sphere. The fraction of CoMs with α angles of less than 90° is larger than 50%; therefore, more than half of the CoMs is present around the half of *Pc* that comprises the hydrophobic patch due to electrostatic preorientation. This

dx.doi.org/10.1021/bi400450q | *Biochemistry* 2013, 52, 6615−6626

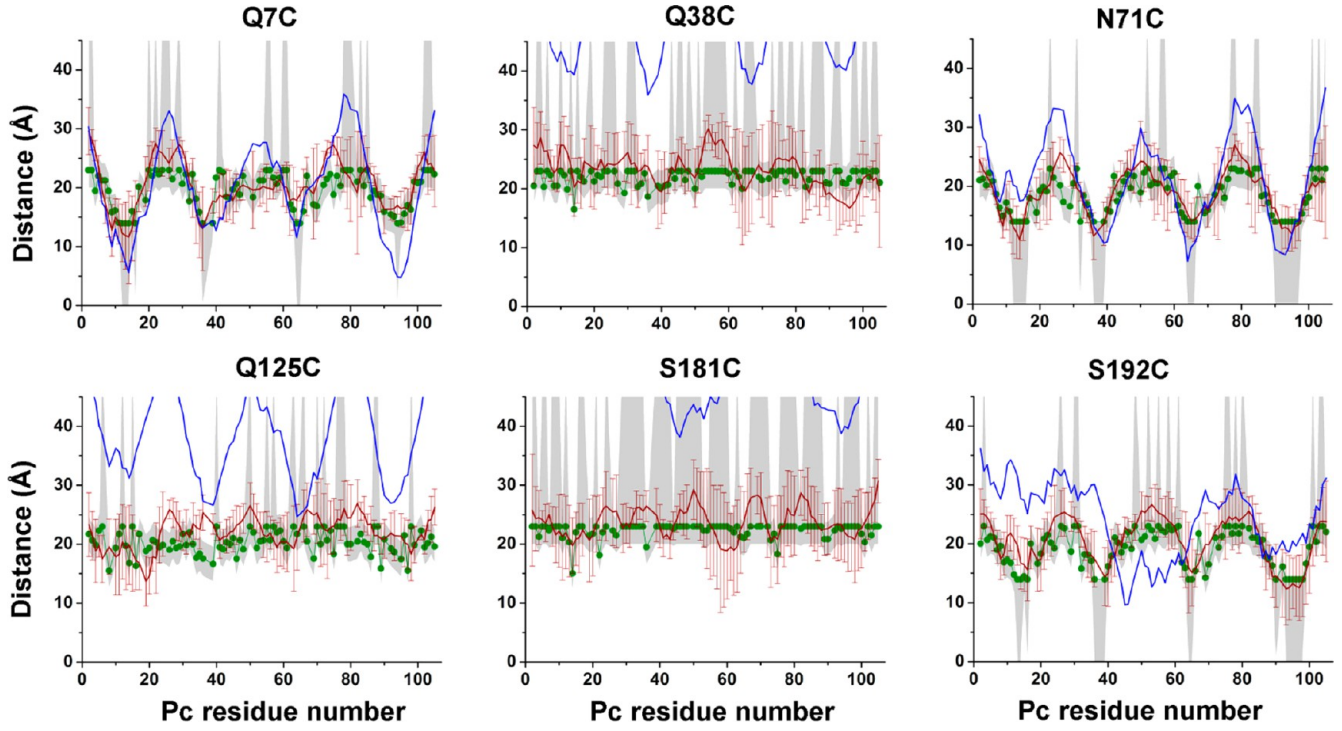

Figure 6. Ensemble docking. Experimental and back-calculated average distances between *Pc* amide protons and oxygen atoms of MTSL conjugated to Cyt *f* are plotted against the *Pc* residue number. The green circles and lines represent the experimental distances, and the gray areas indicate the error margins. The average distances back-calculated from the 20 lowest-energy solutions of the PRE driven ensemble docking are shown as a red line with error bars representing the SD. The average back-calculated distances from the PCS-based final complex models are shown as a blue line. Calculations were performed with $f_1 = 1$.

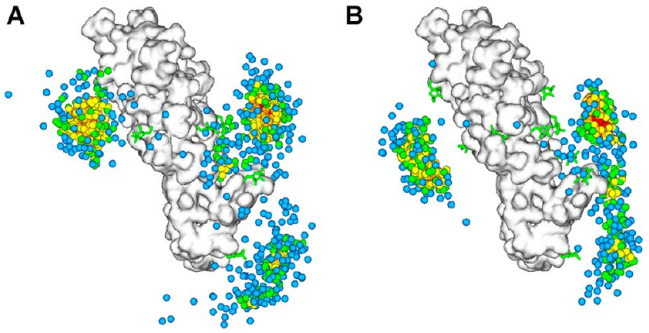

Figure 7. Comparison of the encounter complexes of $^{N\text{-}Ph}$complex (A) and $^{N-N}$complex (B). ^{N}Cyt *f* is shown as a white surface and spin labels as green sticks. *Pc* CoMs are represented by spheres, color-coded to indicate the density of the distributions, decreasing from red to blue. Densities were determined by counting the number of neighbors within 2.5 Å.

suggests that despite the net negative charge of ^{Ph}*Pc*, the localization of positive charges promotes the formation of an oriented complex. For comparison, the same calculations, on the basis of an earlier study,[9] are shown for the $^{N-N}$complex in Figures 8B (gray bars) and 8D. For this complex, the preorientation is stronger and shows a more defined binding spot for $\alpha = 60°-80°$ and $\beta = 30°-120°$. The primary reason for this difference between the complexes of ^{N}Cyt *f* with ^{N}*Pc* and ^{Ph}*Pc* is the presence of two Lys residues (K11 and K20) in this region of ^{N}*Pc*, which are substituted by serine and asparagine, respectively, in ^{Ph}*Pc*.

To compare the importance of ionic strength on the formation of the different Cyt *f*-*Pc* complexes, MC simulations were performed for the $^{N-N}$complex, the $^{N\text{-}Ph}$complex, and the $^{Ph\text{-}Ph}$complex at ionic strength values of 10 mM, 110 mM, and 210 mM (Figure 8E–G). In the cases of the $^{N\text{-}Ph}$complex (Figure 8F) and $^{Ph\text{-}Ph}$complex (Figure 8G), very sparsely distributed encounter complexes were observed at higher values of *I*. For the $^{N-N}$complex (Figure 8E), though the increase in ionic strength resulted in the production of more diffusive encounters, in which the Cyt *f* distribution covers a wider area of the *Pc* surface than observed at low ionic strength, a preferable docking area could be still recognized and related to the electrostatic properties of ^{N}*Pc*. The histograms of the electrostatic interaction energies show that at an ionic strength of 210 mM (green bars), the $^{N\text{-}Ph}$complex (Figure 8F) and $^{Ph\text{-}Ph}$complex (Figure 8G) have lost all electrostatic attraction. For the $^{N-N}$complex (Figure 8E), it is strongly reduced but not completely zero.

Comparison among Cyt *f*-*Pc* Complexes. Recently, we proposed a model for the formation of the $^{N-N}$complex on the basis of the available kinetic and NMR data. Upon approach of the proteins, ^{N}*Pc* is rotated by electrostatic interactions to face ^{N}Cyt *f* with its hydrophobic patch leading to the formation of the encounter complex. This state is stabilized not only by charge interactions but also hydrophobic interactions, allowing a smooth transition from encounter to ET-capable orientations by gradual increase of the hydrophobic overlap and sliding over the hydrophobic interface. It is interesting to interpret the data for the $^{N\text{-}Ph}$complex in light of this model.

The most important difference between ^{N}*Pc* and ^{Ph}*Pc* is the net positive and negative charges, respectively. Given the highly negative charge on ^{N}Cyt *f*, a poor interaction with ^{Ph}*Pc* is expected if charge interactions are dominant. It was found that the affinity is 5-fold lower for ^{Ph}*Pc*, suggesting that charges

dx.doi.org/10.1021/bi400450q | *Biochemistry* 2013, 52, 6615–6626

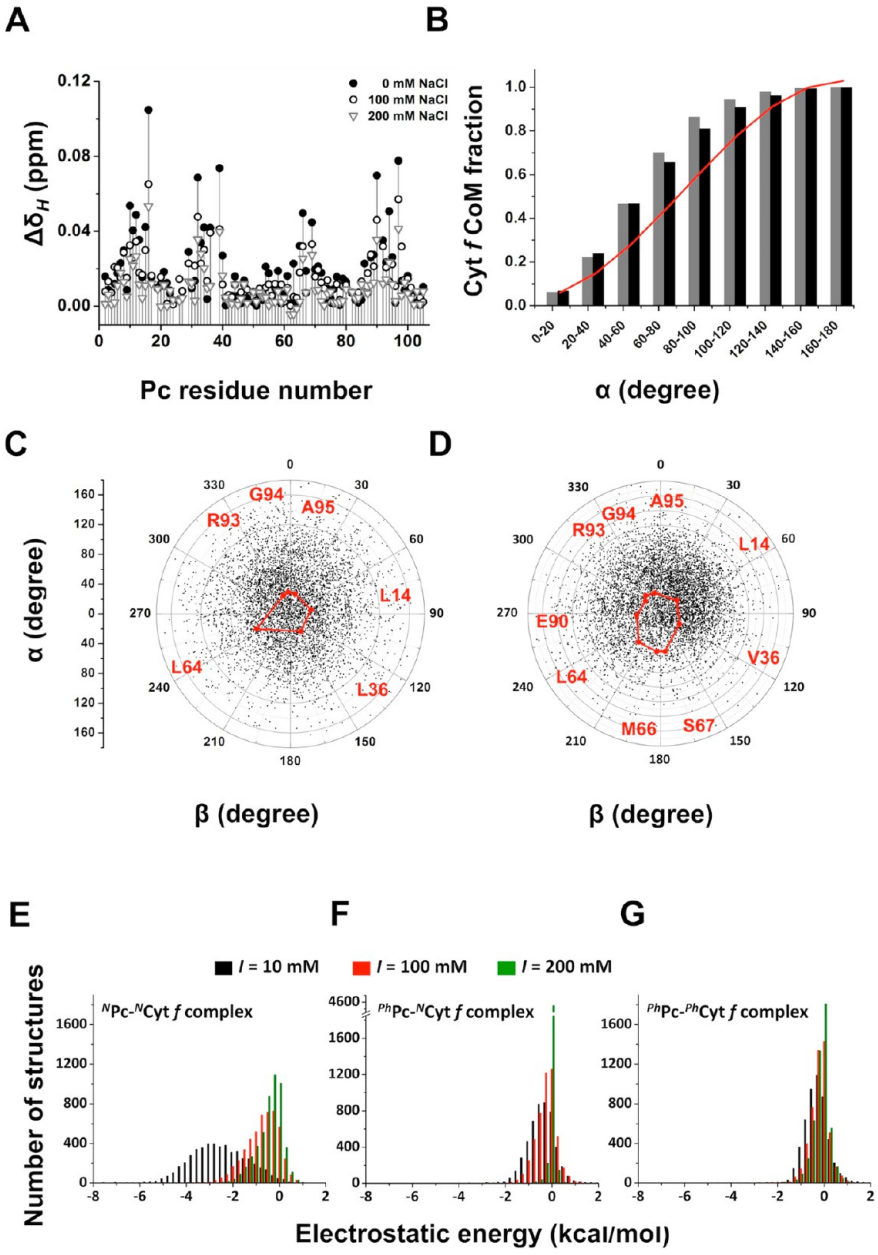

Figure 8. Role of electrostatic interactions in Cyt *f*-*Pc* complexes. (A) Ionic strength dependence of $\Delta\delta_H$ for ^{Ph}Pc backbone amide protons in the presence of reduced ^{N}Cyt *f* at 0 mM NaCl (black dots), 100 mM NaCl (black circles), and 200 mM NaCl (gray triangles). (B,C,D) Analysis of the encounter complex generated by MC simulations. (B) The cumulative fraction of Cyt *f* CoMs for the α angle is plotted for the $^{N\text{-}Ph}$complex (black bars) and $^{N-N}$complex (gray bars). The red line represents the cumulative fraction for a completely random distribution around a sphere. Plots of the position of the ^{N}Cyt *f* CoMs with respect to ^{Ph}Pc (C) and ^{N}Pc (D) in the MC ensembles. The red line connects the positions of hydrophobic patch residues. The Nε of H92 is at the center of the plots in panels C and D. (E,F,G) Electrostatic interaction energy histograms for MC simulations performed at I = 10 mM (black bars), I = 100 mM (red bars), and I = 200 mM (green bars) for $^{N-N}$complexes (E), $^{N\text{-}Ph}$complexes (F), and $^{Ph\text{-}Ph}$complexes (G).

indeed play a role. This is also supported by the MC calculations that show less preorientation for ^{Ph}Pc than for ^{N}Pc. Nevertheless, some preorientation is still observed, indicating that the dipolar nature of the charge distribution is important in complex formation at low ionic strength. The MC results are supported by the CSP and PCS data, which clearly demonstrate that the hydrophobic patch is the side of ^{Ph}Pc that is in contact with ^{N}Cyt *f*. However, the MC results do not agree quantitatively with the PRE data, indicating that electrostatic interactions alone are not sufficient to describe the encounter ensemble and the final complex.

The PCS-based final complex shows predominantly hydrophobic contacts, and the ^{Ph}Pc orientation is different from that in the $^{N-N}$complex, which can be explained by the substitution of several Lys residues on ^{Ph}Pc, resulting in the absence of several charge−charge interactions with negative residues on ^{N}Cyt *f*. The encounter complex produced using PRE-driven ensemble docking is similar to that of the $^{N-N}$complex, though even more diffusive. In both encounter complexes, *Pc* is found in contact with the nonpolar surfaces of Cyt *f*, strongly suggesting that hydrophobic interactions indeed contribute to the encounter complex.

dx.doi.org/10.1021/bi400450q | *Biochemistry* 2013, 52, 6615−6626

The PCS are much smaller in the $^{N\text{-}Ph}$complex than in the $^{N-N}$complex, suggesting that the encounter complex is more populated. The size of PCS strongly depends on the distance between the heme iron and the *Pc* nucleus that experiences the PCS. Thus, it is expected that in the encounter complex, which is spread over a large surface area of Cyt *f*, the PCS will be smaller than that in the final complex. Orientation averaging may reduce the PCS further. The size of the PCS is about 3-fold less for ^{Ph}*Pc* than for ^{N}*Pc* (Figure 3B).

In encounter complexes that are of an electrostatic nature, CSPs are very small, compared to those in the final complex,[40,41] and increasing the fraction of the encounter complex strongly reduces the average size of the CSP in those complexes.[42] The CSPs for ^{Ph}*Pc* in complex with ^{N}Cyt *f* are also reduced compared to those of ^{N}*Pc* (Figure 1C,D) but not by very much, much less than 3-fold. This is an important observation because significant CSPs may be expected also in the encounter complex if it is stabilized by hydrophobic contacts. The chemical shift of amide groups is particularly sensitive to polarity and hydrogen bond formation; therefore, the desolvation of the protein surface that accompanies the formation of hydrophobic contacts is expected to cause significant CSPs.

It is interesting to compare the effects of ionic strength in the $^{N-N}$complex, $^{N\text{-}Ph}$complex, and $^{Ph\text{-}Ph}$complex. The addition of 200 mM NaCl to the $^{Ph\text{-}Ph}$complex (I = 210 mM) had essentially no effect on the fraction of bound *Pc*,[21] suggesting that hydrophobic contacts strongly dominate the interaction. Our simulations are in line with that observation (Figure 8G). The K_D was difficult to determine accurately and was reported to be about 1 mM. Here, we use a range of 1−3 mM. If it is assumed that the hydrophobic contribution to the binding is similar in the three complexes, the contribution of the electrostatic interactions can be estimated for the $^{N-N}$complex and the $^{N\text{-}Ph}$complex. An affinity of 1−3 mM equals a change in free energy of binding of 4.1−3.4 kcal/mol. The K_D values for the $^{N-N}$complex and the $^{N\text{-}Ph}$complex are 80[27] and 400 μM in the absence of salt (I = 10 mM), suggesting an additional contribution from the charge interactions of 1.5−2.2 kcal/mol and 0.55−1.2 kcal/mol, respectively. Thus, the electrostatic interaction represents 27%−38% and 12%−26% of the total binding energy in the $^{N-N}$complex and the $^{N\text{-}Ph}$complex.

The addition of 160 mM NaCl (I = 170 mM) to the $^{N-N}$complex reduced the fraction bound by about 50%,[25] and it can be calculated on the basis of the protein concentrations used in that experiment that the binding energy decreased with 1.6 kcal/mol, nearly abolishing the charge−charge contribution. The same is observed for the $^{N\text{-}Ph}$complex, where the addition of 200 mM NaCl (I = 210 mM) reduces the fraction bound by 60%, which translates to a loss of −0.8 kcal/mol of binding energy under the given experimental conditions. Thus, under the assumption that the hydrophobic contribution is conserved among these complexes, it can be concluded that the electrostatic contribution represents one-third of the binding energy for the $^{N-N}$complex at low ionic strength and much less at more physiological values. For the $^{N\text{-}Ph}$complex, this fraction is even smaller. The trend is qualitatively supported by the electrostatic interaction histograms from the MC calculations (Figure 8E−G). This is an important finding in relation to earlier *in vivo* studies, in which no significant effects of mutation of charged residues in the interface of an algal Cyt *f*-*Pc* complex could be detected in the activity assay.[43,44] These results suggest that charge interactions are not relevant for the complex. However, the results on the cross-complex show that even weak electrostatic interactions are effective in preorienting *Pc* to face Cyt *f* with its hydrophobic patch. Furthermore, many charged residues on both proteins are conserved, especially among plants, suggesting that at least under some circumstances the charge interactions contribute significantly to the electron transfer process in photosynthesis.

In conclusion, the current study fully supports the model complex formation described for the $^{N-N}$complex. In the $^{N\text{-}Ph}$complex, the role of charges has not been abolished at low ionic strength, but it is reduced in favor of hydrophobic contacts, creating a complex with biophysical properties that is a mixture of the $^{N-N}$complex and the $^{Ph\text{-}Ph}$complex. The variation that is observed between mechanisms of complex formation observed for the same complex from different species shows that several ways exist to achieve both fast ET and rapid turnover in protein complexes. The common denominator may be low affinity and low energy barriers between the subsequent states in the reaction.

■ ASSOCIATED CONTENT

Supporting Information

Plot of the average violation of all experimental distances versus the ensemble percentage included in the restraints for the calculations and a comparison of the encounter complexes of the $^{N\text{-}Ph}$complex and $^{N-N}$complex with *Pc* CoMs color-coded according to Cu−Fe distances. This material is available free of charge via the Internet at http://pubs.acs.org.

■ AUTHOR INFORMATION

Corresponding Author

*Phone: +31 (0) 71 527 4628. E-mail: m.ubbink@chem.leidenuniv.nl.

Funding

S.S., M.T., and M.U. received financial support from The Netherlands Organisation for Scientific Research (NWO) and grants 700.57.011 (S.S.) and 700.58.441 (M.T. and M.U.). G.M.U. and J.M.F. were supported by the German Science Foundation (DFG; GRK 1640).

Notes

The authors declare no competing financial interest.

■ ABBREVIATIONS

NMR, nuclear magnetic spectroscopy; *N*, *Nostoc* sp. PCC 7119; *Ph*, *Phormidium laminosum*; Cyt *f*, cytochrome *f*; *Pc*, plastocyanin; ET, electron transfer; MES, 2-(*N*-morpholino) ethanesulfonic acid; HSQC, heteronuclear single quantum coherence; CSP, chemical shift perturbation; PRE, paramagnetic relaxation enhancement; PCS, pseudocontact shift; MTS, (1-acetoxy-2,2,5,5-tetramethyl-δ-3-pyrroline-3-methyl) methanethiosulfonate; MTSL, (1-oxyl-2,2,5,5-tetramethyl-δ-3-pyrroline-3-methyl) methanethiosulfonate; MC, Monte Carlo; CoM, center of mass

■ REFERENCES

(1) Northrup, S. H., and Erickson, H. P. (1992) Kinetics of protein-protein association explained by Brownian dynamics computer simulation. *Proc. Natl. Acad. Sci. U.S.A. 89*, 3338−3342.

(2) Ubbink, M. (2009) The courtship of proteins: understanding the encounter complex. *FEBS Lett. 583*, 1060−1066.

(3) Schreiber, G. (2002) Kinetic studies of protein-protein interactions. *Curr. Opin. Struct. Biol. 12*, 41−47.

(4) Camacho, C. J., Weng, Z., Vajda, S., and DeLisi, C. (1999) Free energy landscapes of encounter complexes in protein-protein association. *Biophys. J. 76*, 1166−1178.
(5) Camacho, C. J., Kimura, S. R., DeLisi, C., and Vajda, S. (2000) Kinetics of desolvation-mediated protein-protein binding. *Biophys. J. 78*, 1094−1105.
(6) Camacho, C. J., and Vajda, S. (2001) Protein docking along smooth association pathways. *Proc. Natl. Acad. Sci. U.S.A. 98*, 10636−10641.
(7) Kim, Y. C., Tang, C., Clore, G. M., and Hummer, G. (2008) Replica exchange simulations of transient encounter complexes in protein-protein association. *Proc. Natl. Acad. Sci. U.S.A. 105*, 12855−12860.
(8) Sugase, K., Dyson, H. J., and Wright, P. E. (2007) Mechanism of coupled folding and binding of an intrinsically disordered protein. *Nature 447*, 1021−1025.
(9) Scanu, S., Foerster, J. M., Ullmann, G. M., and Ubbink, M. (2013) Role of hydrophobic interactions in the encounter cmplex formation of the plastocyanin and cytochrome complex revealed by paramagnetic NMR spectroscopy. *J. Am. Chem. Soc. 135*, 7681−7692.
(10) Hope, A. B. (2000) Electron transfers amongst cytochrome f, plastocyanin and photosystem I: kinetics and mechanisms. *Biochim. Biophys. Acta 1456*, 5−26.
(11) Díaz-Quintana, A., Hervás, M., Navarro, J. A., and De la Rosa, M. A. (2008) Plastocyanin and Cytochrome c_6: The Soluble Electron Carriers between the Cytochrome b_6f Complex and Photosystem I, in *Photosynthetic Protein Complexes: A Structural Approach* (Fromme, P., Ed.), pp 181−200, Wiley-VCH Verlag GmbH & Co. KGaA, Weinheim, Germany.
(12) Crowley, P. B., and Ubbink, M. (2003) Close encounter of the transient kind: protein interactions in the photosynthetic redox chain investigated by NMR spectroscopy. *Acc. Chem. Res. 36*, 723−730.
(13) Schreiber, G., and Fersht, A. R. (1996) Rapid, electrostatically assisted association of proteins. *Nat. Struct. Biol. 3*, 427−431.
(14) Gong, X. S., Wen, J. Q., Fisher, N. E., Young, S., Howe, C. J., Bendall, D. S., and Gray, J. C. (2000) The role of individual lysine residues in the basic patch on turnip cytochrome f for electrostatic interactions with plastocyanin in vitro. *Eur. J. Biochem. 267*, 3461−3468.
(15) Kannt, A., Young, S., and Bendall, D. S. (1996) The role of acidic residues of plastocyanin in its interaction with cytochrome f. *Biochim. Biophys. Acta 1277*, 115−126.
(16) Schlarb-Ridley, B. G., Bendall, D. S., and Howe, C. J. (2002) Role of electrostatics in the interaction between cytochrome f and plastocyanin of the cyanobacterium *Phormidium laminosum*. *Biochemistry 41*, 3279−3285.
(17) Hart, S. E., Schlarb-Ridley, B. G., Delon, C., Bendall, D. S., and Howe, C. J. (2003) Role of charges on cytochrome f from the cyanobacterium *Phormidium laminosum* in its interaction with plastocyanin. *Biochemistry 42*, 4829−4836.
(18) Albarran, C., Navarro, J. A., Molina-Heredia, F. P., Murdoch, P. S., De la Rosa, M. A., and Hervas, M. (2005) Laser flash-induced kinetic analysis of cytochrome f oxidation by wild-type and mutant plastocyanin from the cyanobacterium Nostoc sp. PCC 7119. *Biochemistry 44*, 11601−11607.
(19) Albarran, C., Navarro, J., De la Rosa, M. A., and Hervas, M. (2007) The specificity in the interaction between cytochrome f and plastocyanin from the cyanobacterium Nostoc sp. PCC 7119 is mainly determined by the copper protein. *Biochemistry 46*, 997−1003.
(20) Ubbink, M., Ejdeback, M., Karlsson, B. G., and Bendall, D. S. (1998) The structure of the complex of plastocyanin and cytochrome *f*, determined by paramagnetic NMR and restrained rigid-body molecular dynamics. *Structure 6*, 323−335.
(21) Crowley, P. B., Otting, G., Schlarb-Ridley, B. G., Canters, G. W., and Ubbink, M. (2001) Hydrophobic interactions in a cyanobacterial plastocyanin-cytochrome *f* complex. *J. Am. Chem. Soc. 123*, 10444−10453.
(22) Diaz-Moreno, I., Diaz-Quintana, A., De la Rosa, M. A., and Ubbink, M. (2005) Structure of the complex between plastocyanin and cytochrome f from the cyanobacterium Nostoc sp. PCC 7119 as determined by paramagnetic NMR. The balance between electrostatic and hydrophobic interactions within the transient complex determines the relative orientation of the two proteins. *J. Biol. Chem. 280*, 35784.
(23) Lange, C., Cornvik, T., Diaz-Moreno, I., and Ubbink, M. (2005) The transient complex of poplar plastocyanin with cytochrome f: effects of ionic strength and pH. *Biochim. Biophys. Acta 1707*, 179−188.
(24) Hulsker, R., Baranova, M. V., Bullerjahn, G. S., and Ubbink, M. (2008) Dynamics in the transient complex of plastocyanin-cytochrome f from *Prochlorothrix hollandica*. *J. Am. Chem. Soc. 130*, 1985−1991.
(25) Diaz-Moreno, I., Diaz-Quintana, A., De la Rosa, M. A., Crowley, P. B., and Ubbink, M. (2005) Different modes of interaction in cyanobacterial complexes of plastocyanin and cytochrome f. *Biochemistry 44*, 3176−3183.
(26) Schlarb, B. G., Wagner, M. J., Vijgenboom, E., Ubbink, M., Bendall, D. S., and Howe, C. J. (1999) Expression of plastocyanin and cytochrome f of the cyanobacterium *Phormidium laminosum* in *Escherichia coli* and *Paracoccus denitrificants* and the role of leader peptides. *Gene 234*, 275−283.
(27) Scanu, S., Foerster, J., Finiguerra, M. G., Shabestari, M. H., Huber, M., and Ubbink, M. (2012) The complex of cytochrome f and plastocyanin from Nostoc sp. PCC 7119 is highly dynamic. *ChemBioChem 13*, 1312−1318.
(28) Milikisyants, S., Scarpelli, F., Finiguerra, M. G., Ubbink, M., and Huber, M. (2009) A pulsed EPR method to determine distances between paramagnetic centers with strong spectral anisotropy and radicals: the dead-time free RIDME sequence. *J. Magn. Reson. 201*, 48−56.
(29) Delaglio, F., Grzesiek, S., Vuister, G. W., Zhu, G., Pfeifer, J., and Bax, A. (1995) NMRPipe: a multidimensional spectral processing system based on UNIX pipes. *J. Biomol. NMR 6*, 277−293.
(30) Vranken, W. F., Boucher, W., Stevens, T. J., Fogh, R. H., Pajon, A., Llinas, M., Ulrich, E. L., Markley, J. L., Ionides, J., and Laue, E. D. (2005) The CCPN data model for NMR spectroscopy: development of a software pipeline. *Proteins 59*, 687−696.
(31) Battiste, J. L., and Wagner, G. (2000) Utilization of site-directed spin labelling and high-resolution heteronuclear nuclear magnetic resonance for global fold determination of large proteins with limited nuclear overhauser effect data. *Biochemistry 39*, 5355−5365.
(32) Baniulis, D., Yamashita, E., Whitelegge, J. P., Zatsman, A. I., Hendrich, M. P., Hasan, S. S., Ryan, C. M., and Cramer, W. A. (2009) Structure-function, stability, and chemical modification of the cyanobacterial cytochrome b6f complex from Nostoc sp. PCC 7120. *J. Biol. Chem. 284*, 9861−9869.
(33) Banci, L., Bertini, I., Cavallaro, G., Giachetti, A., Luchinat, C., and Parigi, G. (2004) Paramagnetism-based restraints for Xplor-NIH. *J. Biomol. NMR 28*, 249−261.
(34) Schwieters, C. D., Kuszewski, J. J., Tjandra, N., and Clore, G. M. (2003) The Xplor-NIH NMR molecular structure determination package. *J. Magn. Reson. 160*, 65−73.
(35) Ullmann, G. M., Knapp, E. W., and Kostic, N. M. (1997) Computational simulation and analysis of dynamic association between plastocyanin and cytochrome f. Consequences for the electron-transfer reaction. *J. Am. Chem. Soc. 119*, 42−52.
(36) Bashir, Q., Volkov, A. N., Ullmann, G. M., and Ubbink, M. (2010) Visualization of the encounter ensemble of the transient electron transfer complex of cytochrome c and cytochrome c peroxidase. *J. Am. Chem. Soc. 132*, 241−247.
(37) Ubbink, M., Lian, L. Y., Modi, S., Evans, P. A., and Bendall, D. S. (1996) Analysis of the 1H-NMR chemical shifts of Cu(I)-, Cu(II)- and Cd-substituted pea plastocyanin. Metal-dependent differences in the hydrogen-bond network around the copper site. *Eur. J. Biochem. 242*, 132−147.
(38) Carrell, C. J., Schlarb, B. G., Bendall, D. S., Howe, C. J., Cramer, W. A., and Smith, J. L. (1999) Structure of the soluble domain of cytochrome f from the cyanobacterium *Phormidium laminosum*. *Biochemistry 38*, 9590−9599.

(39) Clore, G. M., and Iwahara, J. (2009) Theory, practice and applications of paramagnetic relaxation enhancement for the characterization of transient low-population states of biological macromolecules and their complexes. *Chem. Rev. 109*, 4108−4139.
(40) Worrall, J. A. R., Liu, Y. J., Crowley, P. B., Nocek, J. M., Hoffman, B. M., and Ubbink, M. (2002) Myoglobin and cytochrome b5: a nuclear magnetic resonance study of a highly dynamic protein complex. *Biochemistry 41*, 11721−11730.
(41) Xu, X. F., Reinle, W. G., Hannemann, F., Konarev, P. V., Svergun, D. I., Bernhardt, R., and Ubbink, M. (2008) Dynamics in a pure encounter complex of two proteins studied by solution scattering and paramagnetic NMR spectroscopy. *J. Am. Chem. Soc. 130*, 6395−6403.
(42) Volkov, A. N., Bashir, Q., Worrall, J. A. R., Ullmann, G. M., and Ubbink, M. (2010) Shifting the equilibrium between the encounter state and the specific form of a protein complex by interfacial point mutations. *J. Am. Chem. Soc. 132*, 11487−11495.
(43) Soriano, G. M., Ponamarev, M. V., Tae, G. -S., and Cramer, W. A. (1996) Effect of the interdomain basic region of cytochrome f on its redox reactions in vivo. *Biochemistry 35*, 14590−14598.
(44) Soriano, G. M., Ponamarev, M. V., Piskorowski, R. A., and Cramer, W. A. (1998) Identification of the basic residues of cytochrome f responsible for electrostatic docking interactions with plastocyanin in vitro: relevance to the electron transfer reaction in vivo. *Biochemistry 37*, 15120−15128.